CHAPTER IV
RESULTS AND DISCUSSION

4.1 Validation of FLUENT CFD Model

Flow visualization and pressure measurement have been done to validate the CFD model. The results were compared with those from CFD simulation. FLUENT 6.3 is the CFD software used for simulation.

4.1.1 Flow Visualization

In this experiment, bubble and dye were used as a tracer to track the movement of the flow near scalloped surface. By using a high speed camera, the hydrodynamics near scalloped surface can be tracked. In Figure 4.1, the video of flow hydrodynamics using bubble technique was caught by high speed camera.

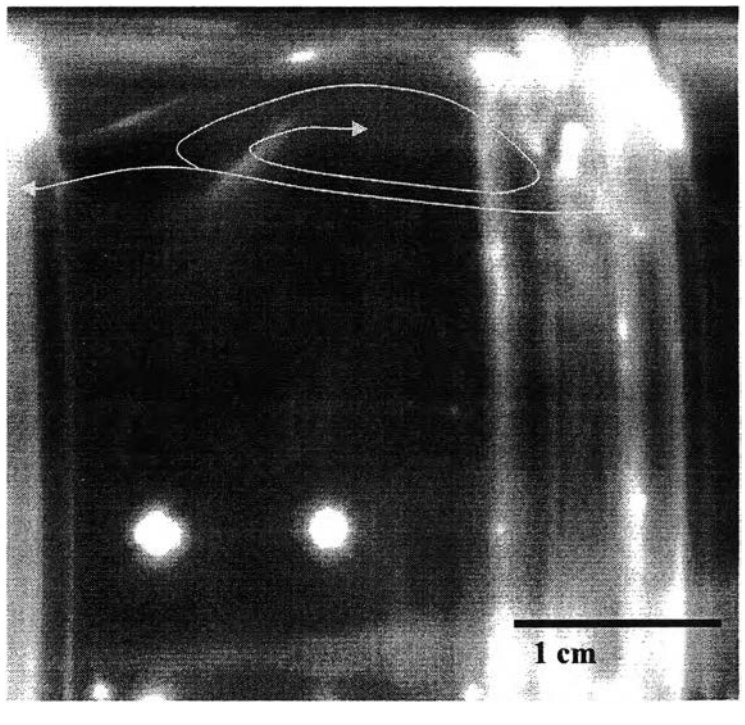

Figure 4.1 Picture from high speed camera

The bubble size is very small until it looks like a white fine particle. Since the bubble is very fine, the buoyancy force is minimized and it is reasonable to

assume that the bubble move along with flow at the same velocity and direction. The flow separation and recirculation were clearly observed. The flow path of the bubble is shown in Figure 4.1.

Food color dye was also be used as a tracer to visualize the flow hydrodynamics near scalloped surface. Because of its high diffusion rate, the flow path cannot be clearly seen. After the dye was mixed with milk to decrease diffusion rate, the result is better but still not good.

The stream line can be visualized by using low shutter speed technique. When shutter speed is low, the pathways of bubbles turn in to a line. Figure 4.2 shows the stream line caught by low shutter speed technique.

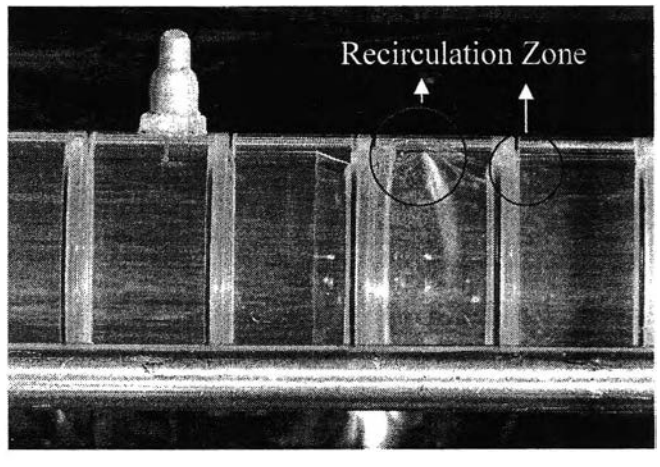

Figure 4.2 Stream line visualized by low shutter speed technique

There are two recirculation zone observed, one is at the bottom of the scallop, another one is at the end of the scallop when the diameter is expanding. The stream line is clearly seen by bubble technique.

4.1.2 Pressure Measurement

The wall static pressure along the pipe was measured with a very sensitive pressure transducer. Due to turbulence, high pressure fluctuation was observed on the pressure transducer's meter. Because of this fluctuation, it is not easy to read the exact value of static pressure. High shutter speed camera was used to solve this problem by taking a picture of the value on the meter at certain number of

time and an average value are used to represent the data. The pressure transducer is shown in figure 4.3.

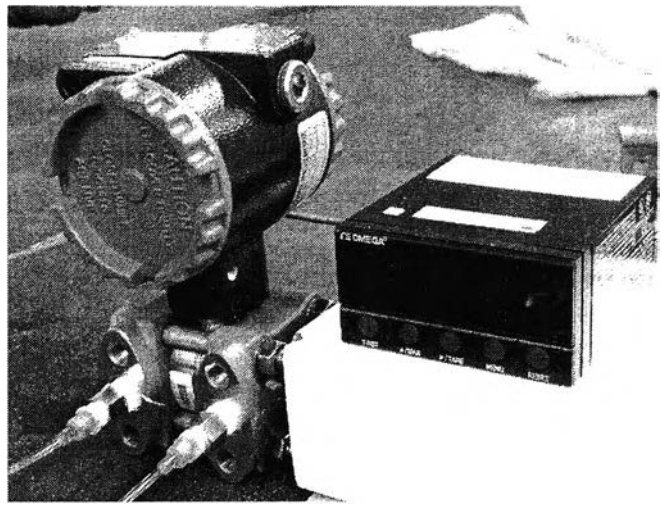

Figure 4.3 Pressure transducer and its meter

The temperature was controlled to be constant at 25°C by adjusting the flow rate of cooling water. The relative wall static pressure along the pipe of one scallop from the flow rate of 6, 9, 12, 15 and 18 GPM are shown in Figure 4.4, 4.5, 4.6, 4.7 and 4.8 respectively. The result for two scallop test section is shown in Figure 4.9. The high fluctuation around scallop area was observed.

The reference point is the end of the pipe which the value of static pressure equal zero. The higher flow rate, the more wall static pressure drops.

From the experimental results, changes in wall static pressure results from changes in geometry. Before the flow reach scallop, the pressure constantly decreases. When it reaches scallop, the pressure goes up a little bit because the flow starts to be compressed. After that, the diameter decrease causing the flow to have higher velocity and the wall static pressure start decrease dramatically. The wall static pressure hit the lowest point at the crest of scallop and starts to increase again when the diameter increase. The wall static pressure hit the highest point for a second time at the area of flow impingement, at the average diameter of the test section, and then it starts to decrease due to the decrease in diameter and hit the valley at the crest of scallop. After that it starts to increase again result from the increase in diameter.

Finally, the wall static pressure constantly decreases again due to the wall friction loss, which is the same trend as before it reaches the scallop.

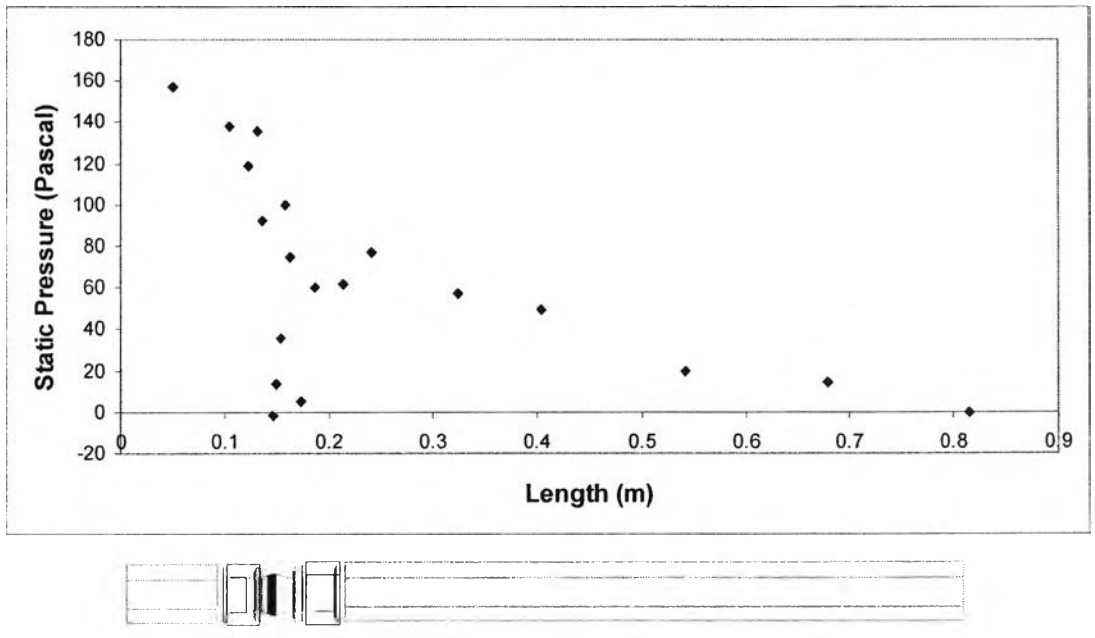

Figure 4.4 The wall static pressure along the pipe at 6 GPM, 1 scallop

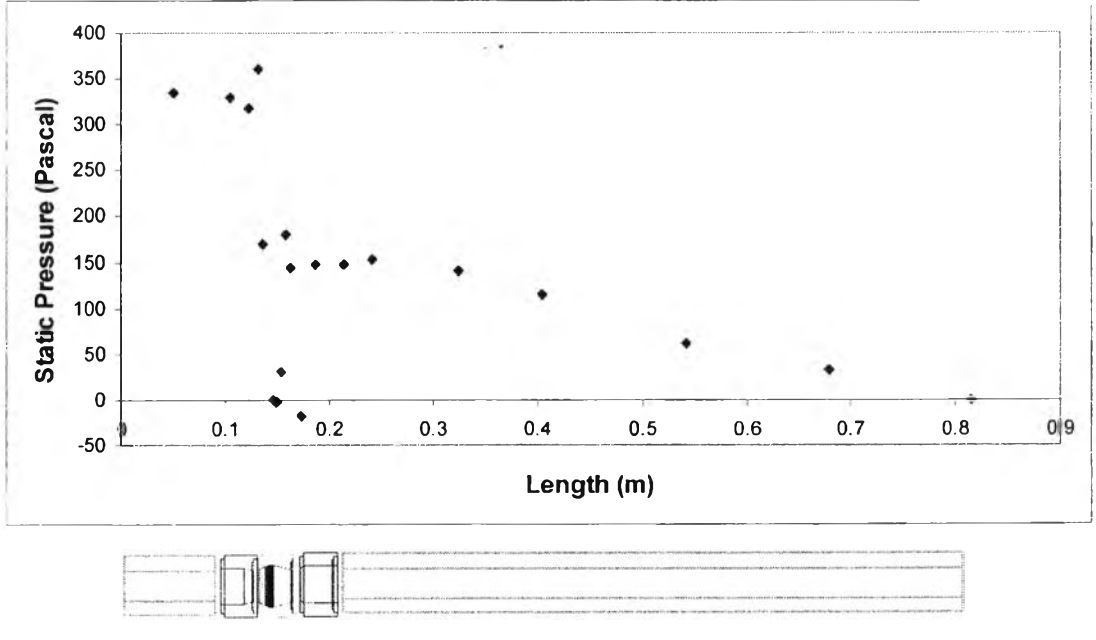

Figure 4.5 The wall static pressure along the pipe at 9 GPM, 1 scallop

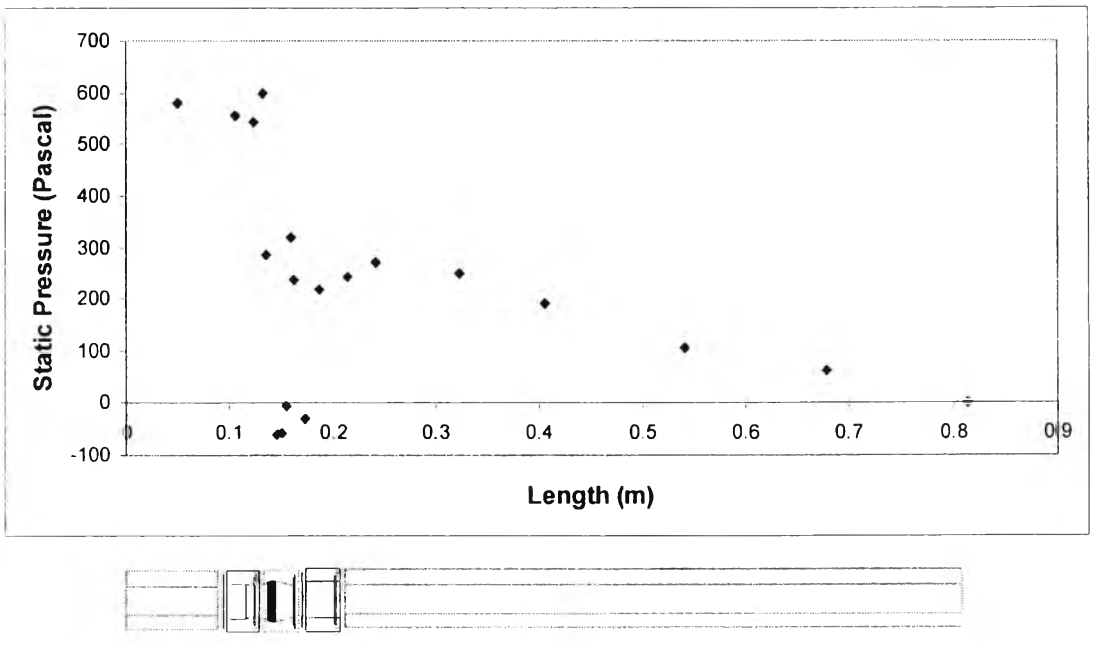

Figure 4.6 The wall static pressure along the pipe at 12 GPM, 1 scallop

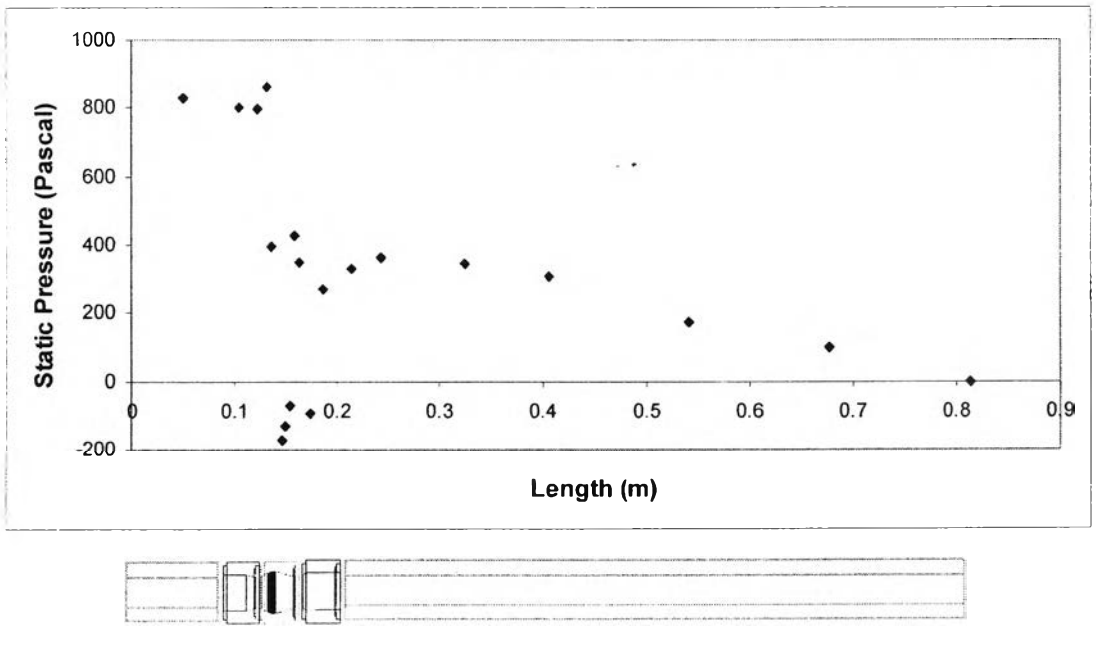

Figure 4.7 The wall static pressure along the pipe at 15 GPM, 1 scallop

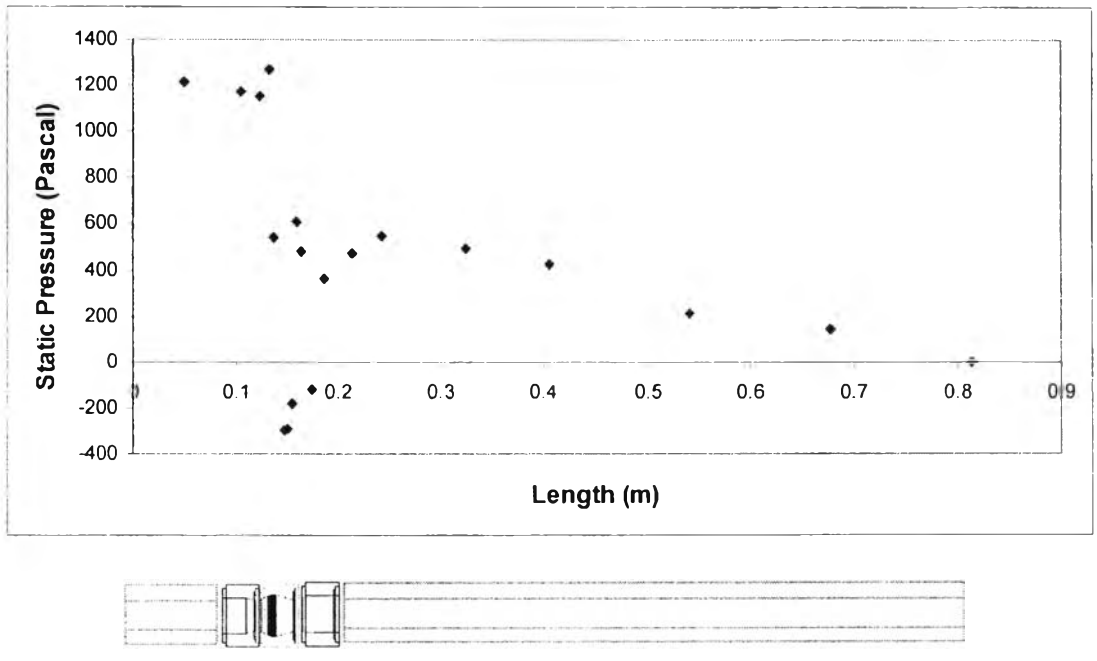

Figure 4.8 The wall static pressure along the pipe at 18 GPM, 1 scallop

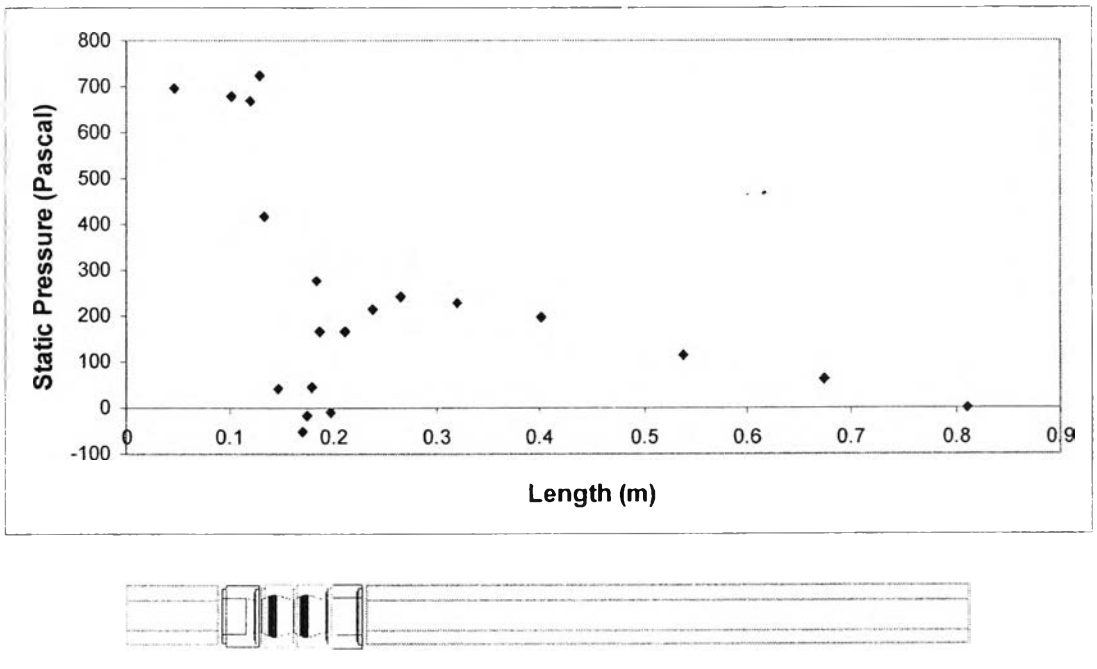

Figure 4.9 The wall static pressure along the pipe at 12 GPM, 2 scallops

The results from flow visualization and static pressure measurement will be used to validate the CFD simulation and the most appropriate viscous model for flow near scalloped surface will be investigated in section 2.1.3.

4.1.3 CFD Simulation and Viscous Model Selection with FLUENT

FLUENT 6.3 is used for CFD simulation. Mesh was generated using GAMBIT, mesh generating software. FLUENT has provided a numerical solver that solves the transport equation at any node on the mesh. So, mesh quality also affects the accuracy of the simulation. In order to get an accurate prediction, mesh should be fine enough until the solution is not a function of mesh resolution. Figure 4.10 and Figure 4.11 illustrate mesh independent study.

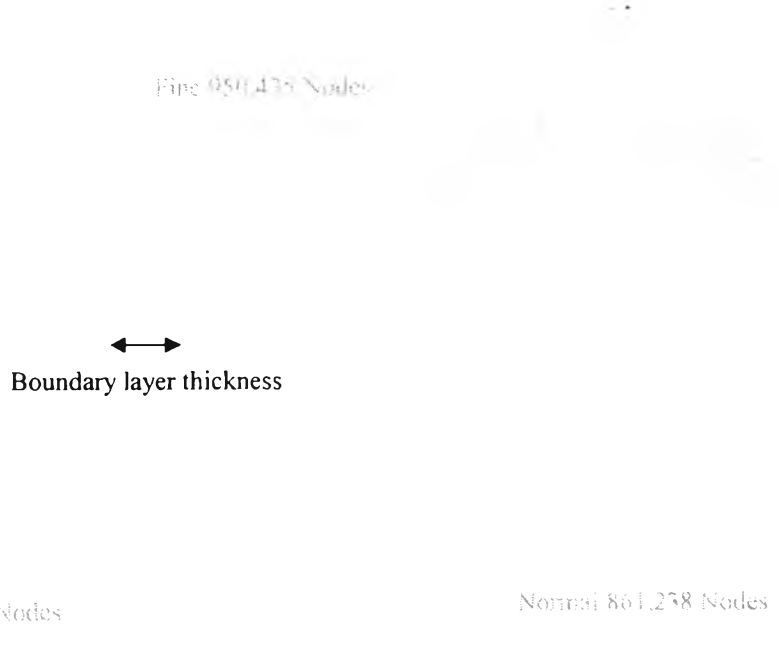

Figure 4.10 Mesh's resolution on the cross section area of the pipe

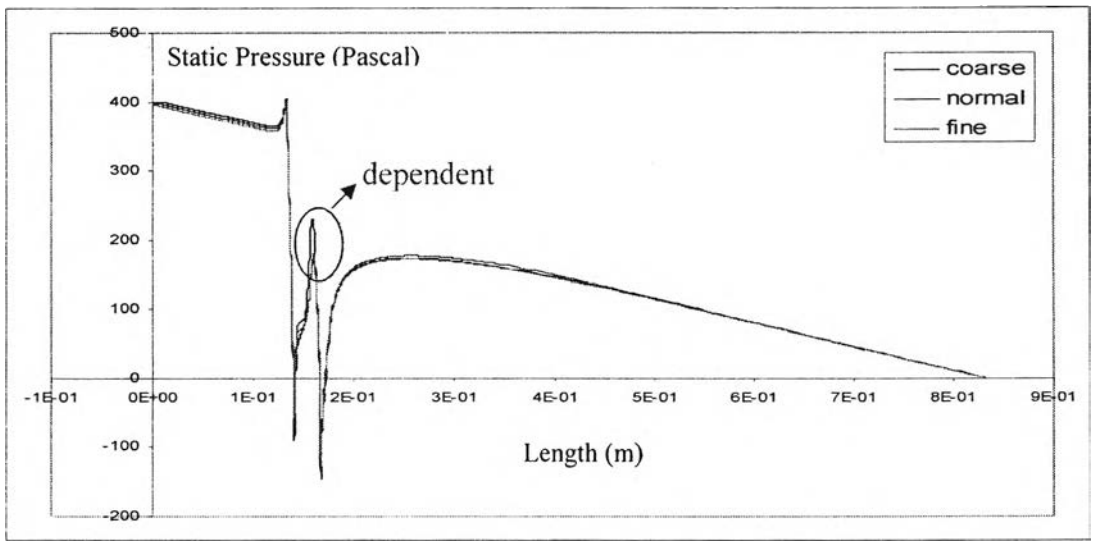

Figure 4.11 Mesh independent study shows that the solution of the coarse mesh still depends on the mesh resolution and the most appropriate mesh is the normal resolution mesh which has 861,238 nodes.

The mainly difference among each mesh is the resolution of the boundary layer. To get an accurate solution, the mesh's boundary layer thickness is equal to the combination of lamina sub layer thickness and transient thickness in turbulence flow. The difference in mesh resolution can affect the solution as shown in Figure 4.11. The coarse mesh is not good because the solution still change with increasing in resolution. The normal mesh is the best mesh since the solution doesn't change when the resolution is increase and it requires less computational resource than the finer one.

Second order with double precision calculation is always used in the simulation in order to get very accurate results. Figure 4.12 shows the difference between the solutions from first order and second order calculation. Solution from first order calculation has more numerical diffusion. It is obvious that the problem set up play an important role to the simulation results.

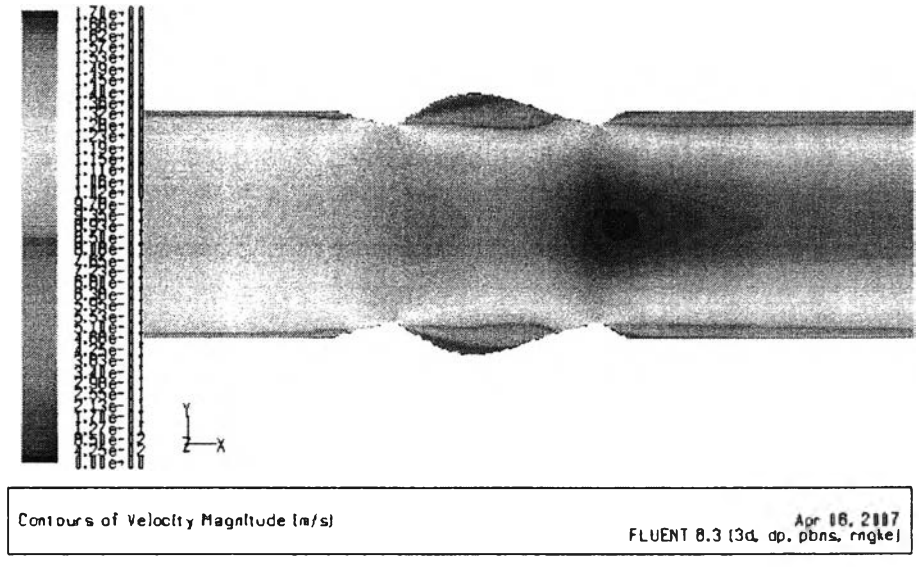

Results from First Order Calculation

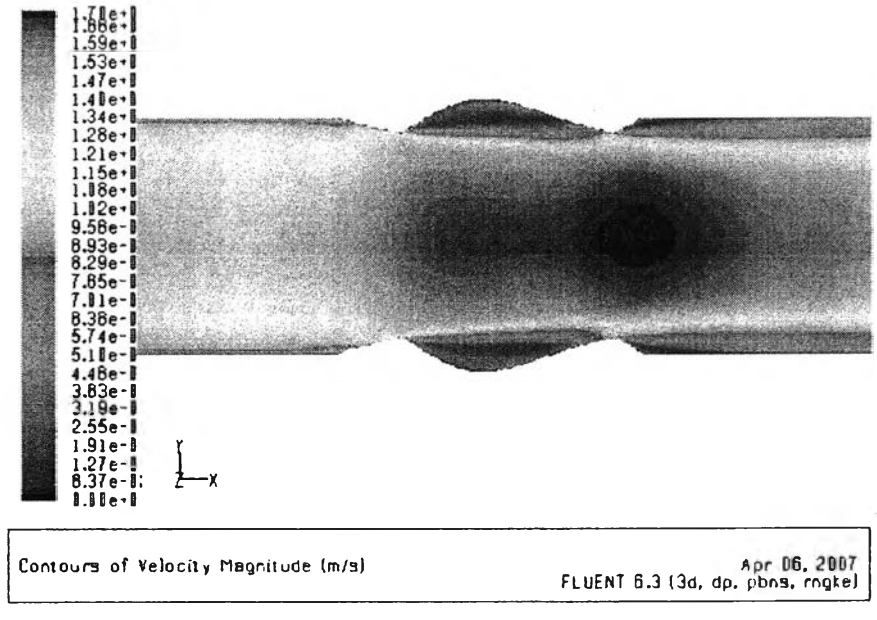

Results from Second Order Calculation

Figure 4.12 Comparison of the results from first and second order calculation

In order to compare with the experimental results and validate the CFD model, the simulation using RNG k-ε, SST k-ω and R k-ε viscous model at

various flow rates have been simulated. The comparison at 6, 9, 12, 15 and 18 GPM are shown in Figure 4.13, 4.14, 4.15, 4.16 and 4.17 respectively.

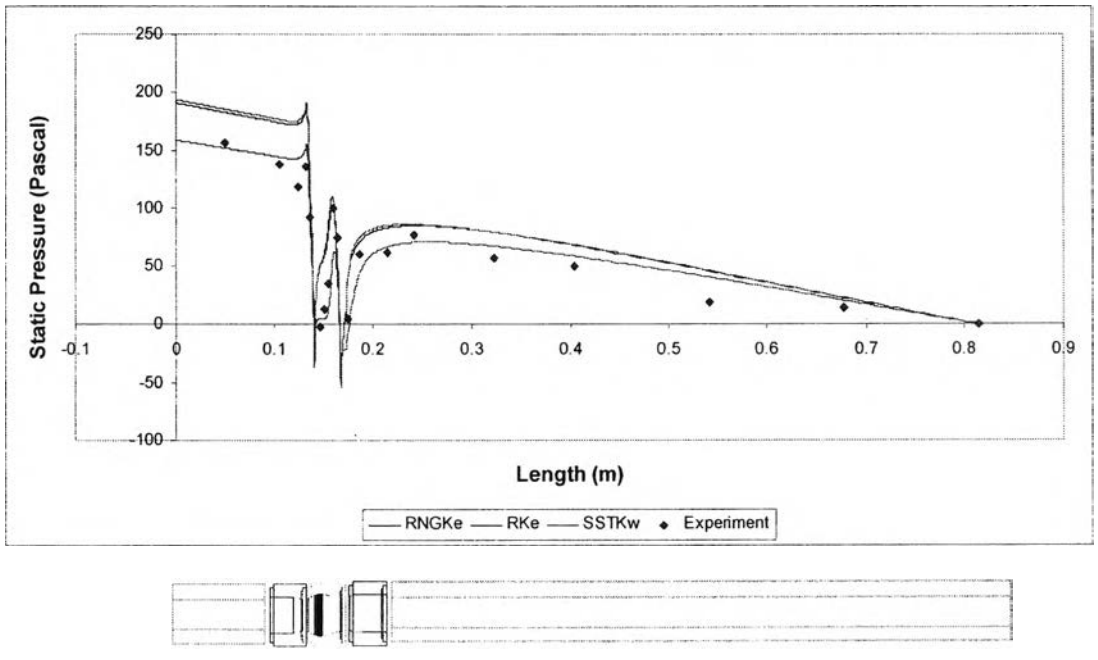

Figure 4.13 Comparison of viscous models at 6 GPM

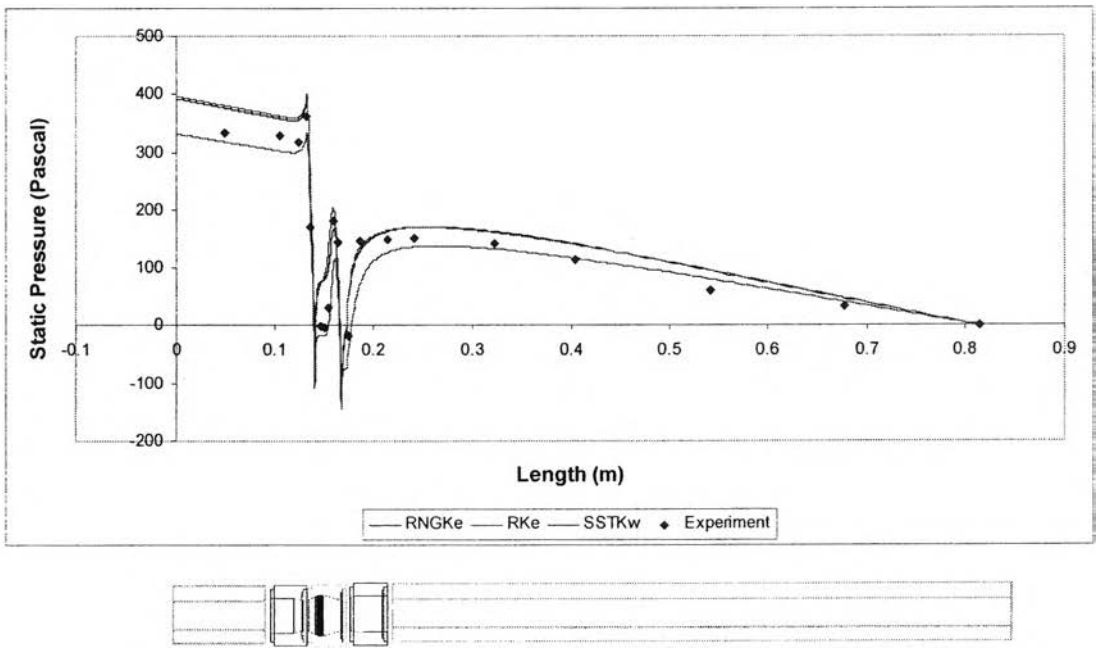

Figure 4.14 Comparison of viscous models at 9 GPM

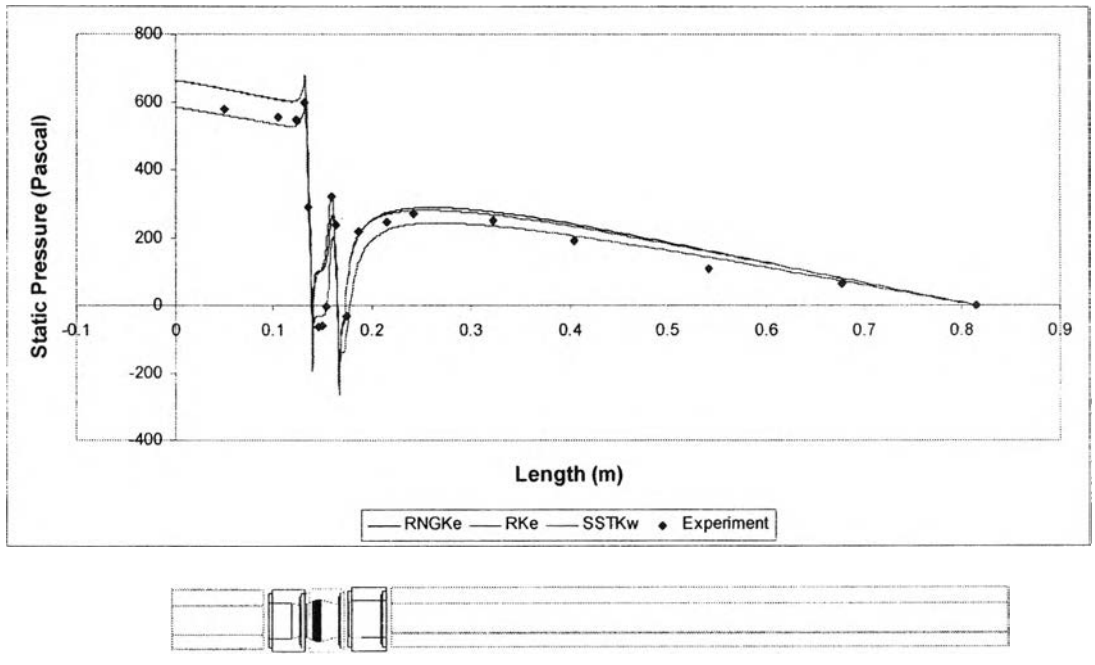

Figure 4.15 Comparison of viscous models at 12 GPM

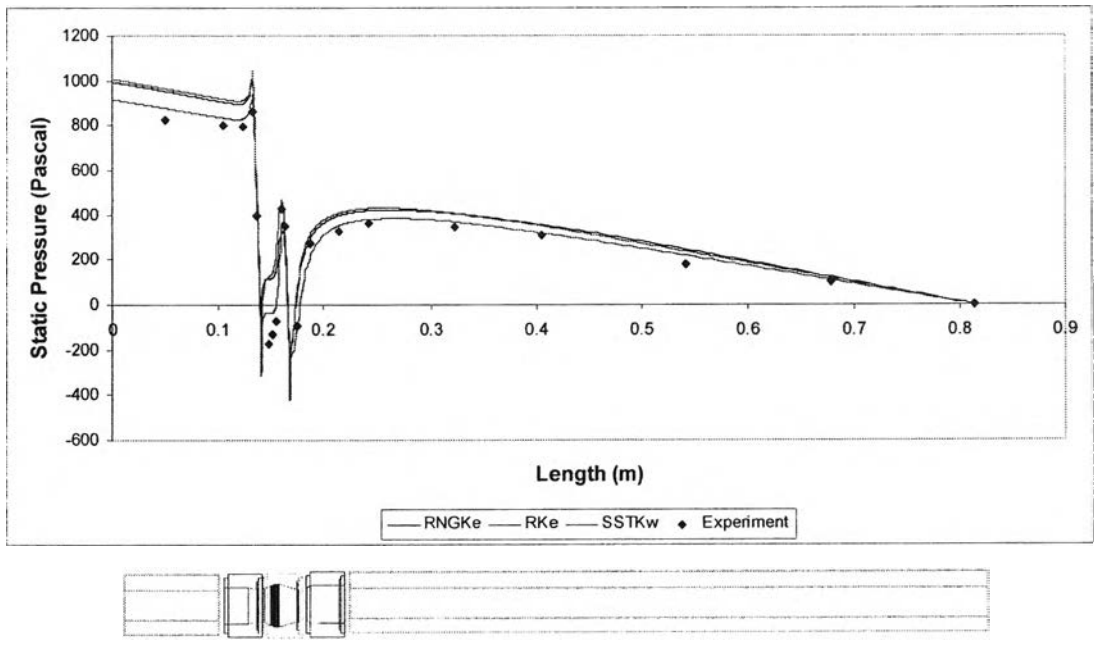

Figure 4.16 Comparison of viscous models at 15 GPM

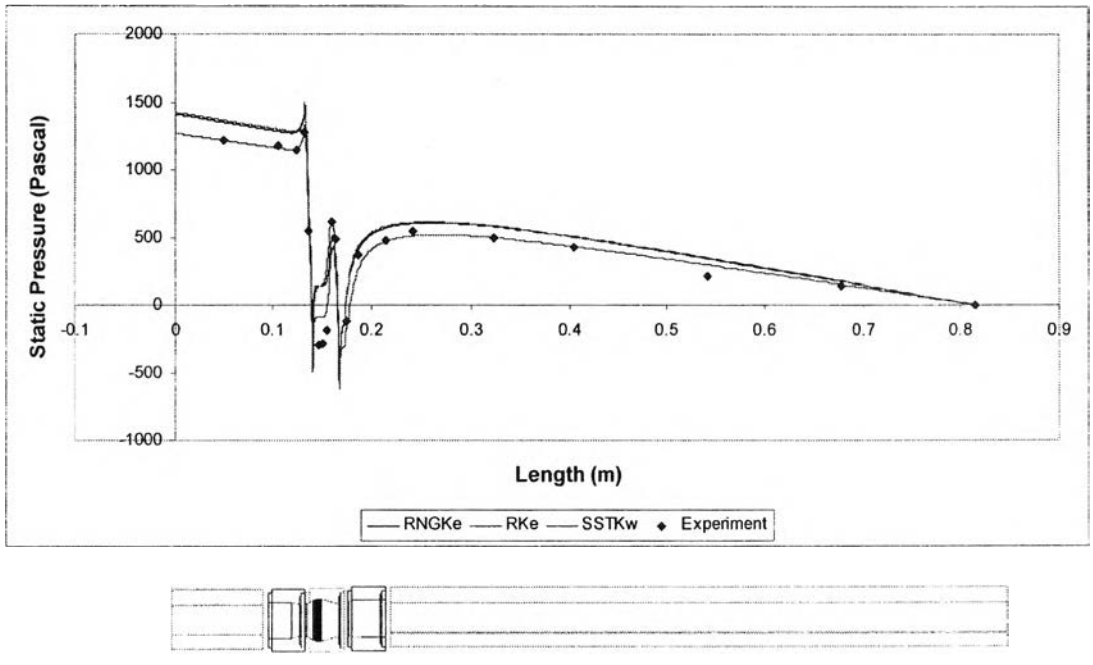

Figure 4.17 Comparison of viscous models at 18 GPM

It is obvious that SST k-ω viscous model provide the most accurate prediction of flow hydrodynamics near scalloped surface. The other two model over predict the wall static pressure especially around the recirculation zone. Anyway, RNG k-ε and R k-ε model give a better prediction of wall static pressure near the crest.

SST k-ω viscous model was tested again with 2 scallop geometry at 12 GPM as shown in Figure 4.18. The result is well match with the experimental results. So, it is reasonable to consider that FLUENT CFD model for the flow near scalloped surface was validated quantitatively and the best viscous model for this type of geometry is SST k-ω viscous model.

The velocity and pressure contour simulated by FLUENT at 9 GPM were shown in figure 4.19. Recirculation zone can be observed in the velocity contour which is on congruence with experimental results. The flow path illustrated in figure 4.20 is close to the one from flow visualization experiment. Then, the FLUENT CFD model was validated qualitatively.

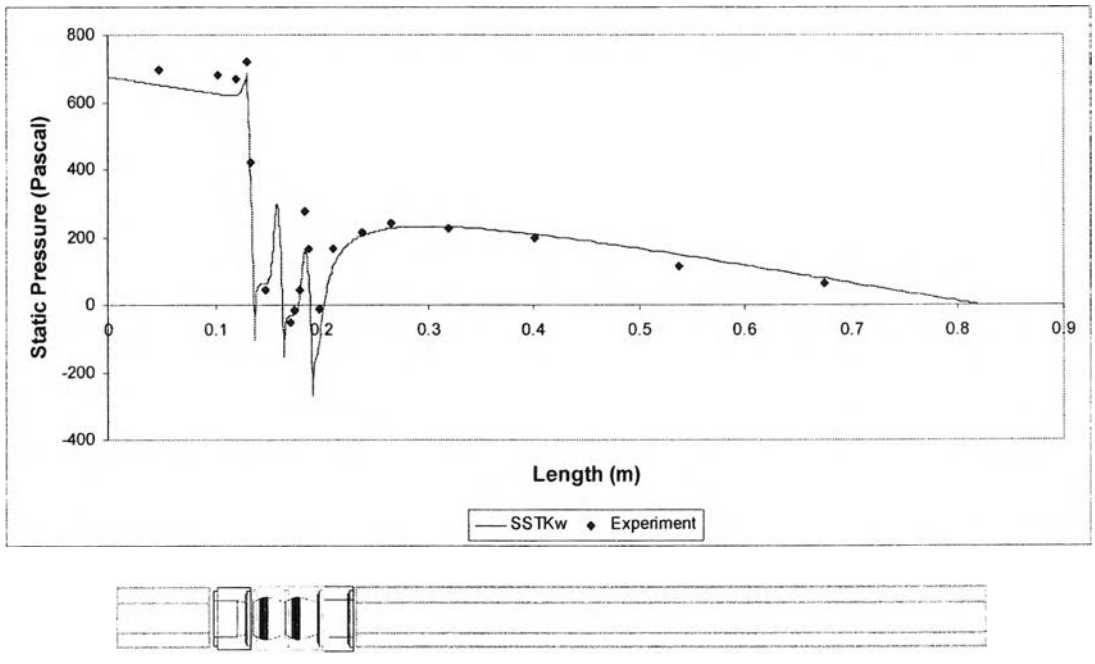

Figure 4.18 Prediction of SST k-ω at 12 GPM, 2 scallops

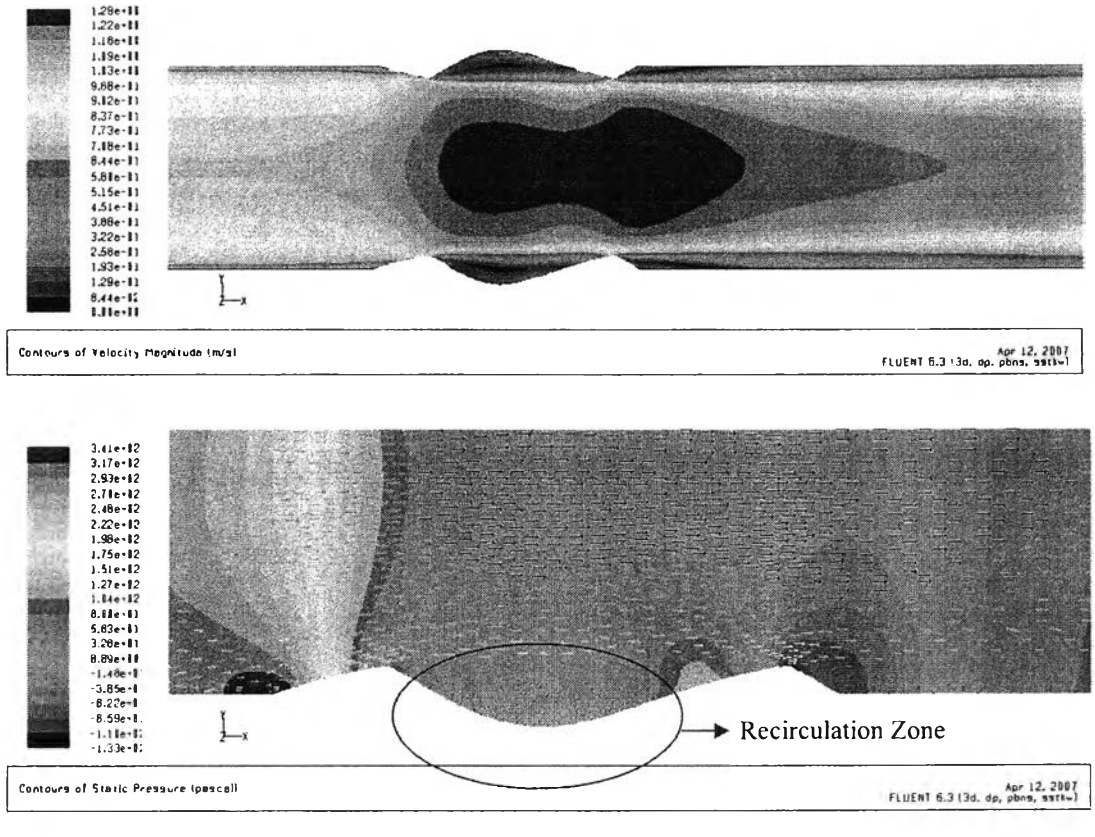

Figure 4.19 Velocity and pressure contour at 9 GPM, SST k-ε model

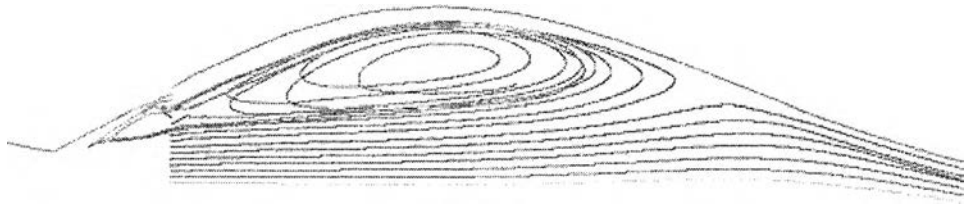

Figure 4.20 Flow path line near scalloped surface

4.2 Effect of Scallop's Surface Area to the Pressure Drop

4.2.1 Effect of Scallop's Surface Area with Forward Flow Direction

In this experiment, the flow is in the forward direction as shown in figure 4.21. The scallop's surface area was varied while the pressure drop was measured. The number of scallop increase from 0 to 15 pieces and the pressure drop between the beginning and the end of test section was measured with high sensitive pressure transducer.

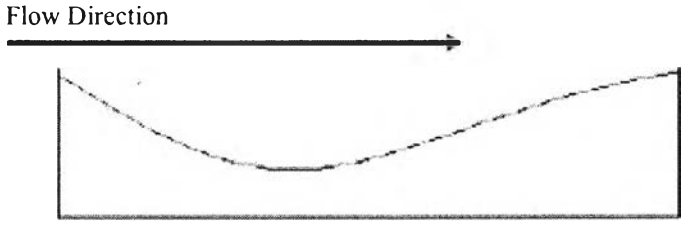

Figure 4.21 Forward flow direction

The effect of scallop surface area is shown in Figure 4.22. The increase in surface area is proportional to the increase in pressure drop. Figure 4.23 shows that the pressure drop is proportional to square of Reynolds number. It is noticed that this kind of surface geometry behave like a regular surface roughness since the wall head lost (or pressure drop) is proportional to the length (or surface area) and velocity (or Reynolds number) square as describe by the equation below.

$$h_f = \frac{\Delta p}{\rho g} = f\frac{L}{d}\frac{V^2}{2g} \approx 0.316\left(\frac{\mu}{\rho V d}\right)^{1/4}\frac{L}{d}\frac{V^2}{2g} \qquad (4.1)$$

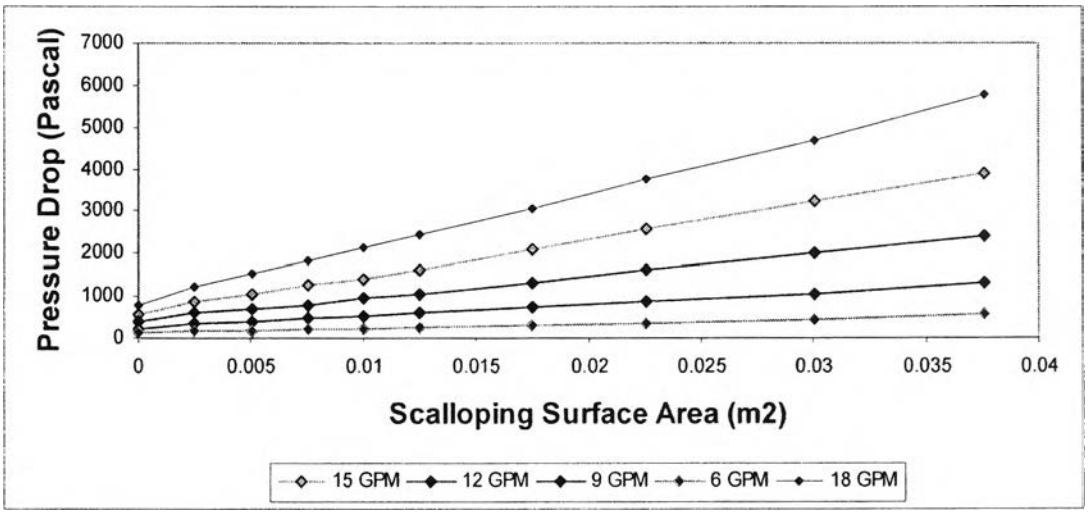

Figure 4.22 The pressure drop increase constantly with the scallop's surface area for forward flow direction.

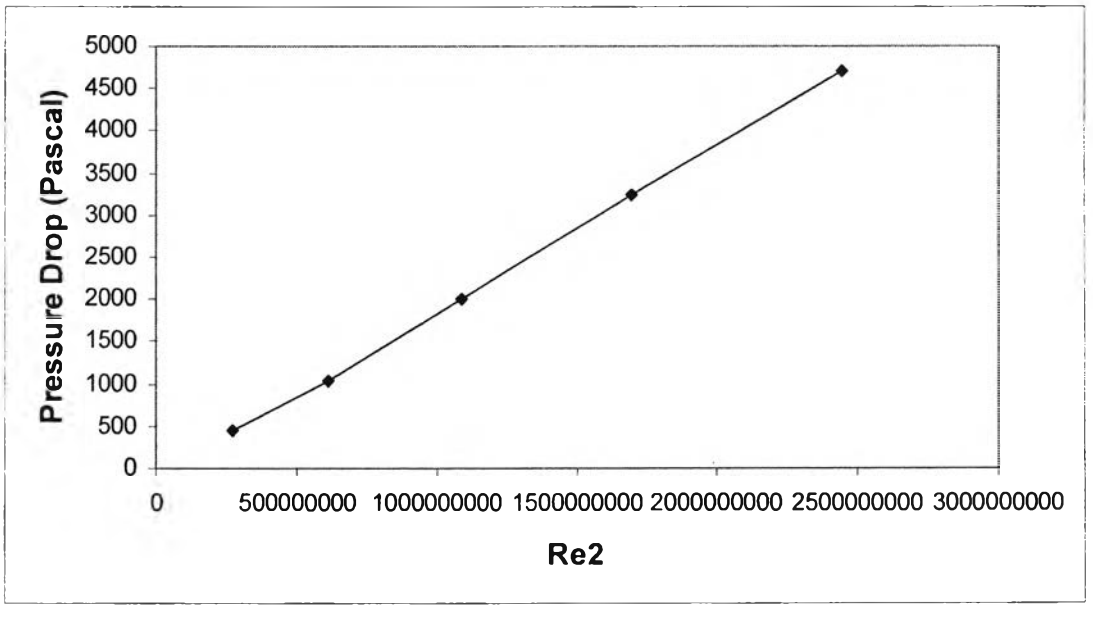

Figure 4.23 The pressure drop is proportional to Reynolds number square for forward flow direction.

The velocity and pressure contour for 5 scallops test section with forward flow are illustrated in appendix A.

4.2.2 Effect of Scallop's Surface Area with Backward Flow Direction

Repeat the experiment from 2.2.1 but backward flow direction. The scheme of the flow in backward direction is shown in figure 4.24.

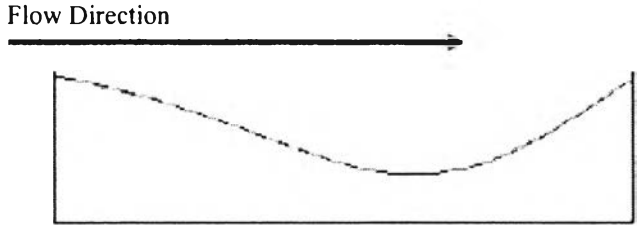

Figure 4.24 Backward flow direction

From Figure 4.25 and 4.26, it can be concluded that scalloped surface also behave like a regular roughness in backward flow direction. The velocity and pressure contour for 1 and 5 scallops test section with backward flow are illustrated in appendix A.

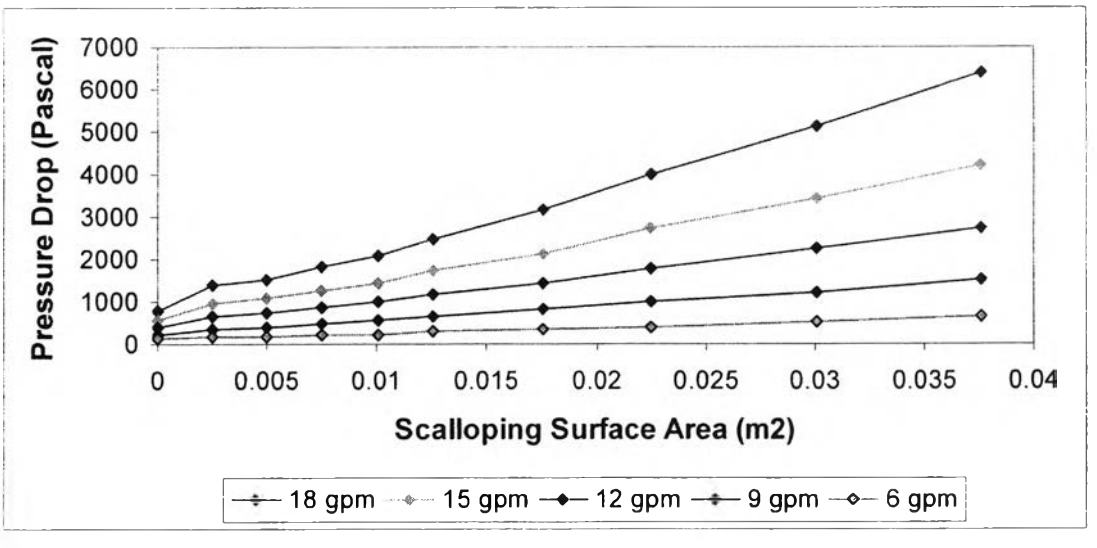

Figure 4.25 The pressure drop increase constantly with the scallop's surface area for backward flow direction.

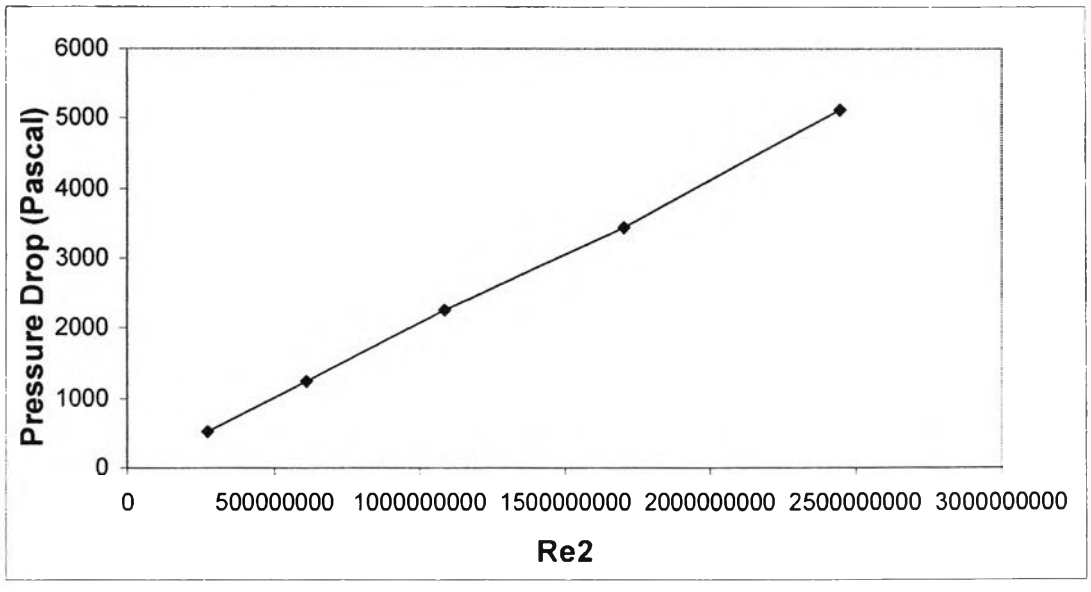

Figure 4.26 The pressure drop is proportional to Reynolds number square for backward flow direction.

4.2.3 Comparison of Friction Factor

The friction factor for both forward and backward flow direction was calculated by equation 4.1. The results were shown in figure 4.27.

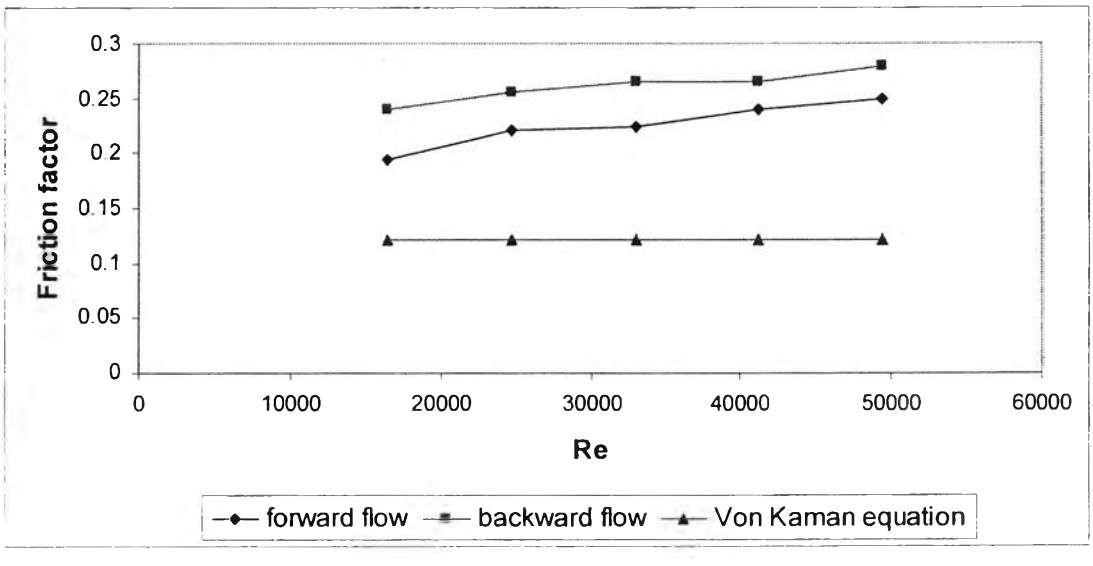

Figure 4.27 The friction factors from the experiment are compared with the one calculated from Von Kaman equation.

The friction factor calculated from the experiment are not equal to the one calculated from Von Kaman equation for fully rough in turbulence flow which give a constant value of friction factor at any Re. The friction factor calculated from the experiment still depends on the Reynolds number of flow. Von Kaman equation is described below.

$$\frac{1}{f^{1/2}} = -2.0 \log \frac{\epsilon/d}{3.7} \qquad \text{fully rough flow} \tag{4.2}$$

It can be noticed that the friction factors obtained from backward and forward flow are not the same even though they have the same roughness height. So, it can be implied that the Von Kaman equation and Moody chart cannot applied to this type of roughness. The correlation is needed to obtain the realistic value.

4.3 Effect of Scallop's Distribution on Pressure Drop

The scallop pieces were arranged in many patterns and the effect of their distribution were investigated.

From figure 4.28, at the same number of scallop pieces, the pressure drop is almost the same regardless how they were arranged. It can be deducted that the pressure drop mainly depends on the surface geometry, not the position. The pressure drop of scalloped surface depends on the scallop's surface area and is almost not affected by the scallop's distribution.

The 3D scalloped surface experiment should be conducted to confirm the results from 2D scalloped surface.

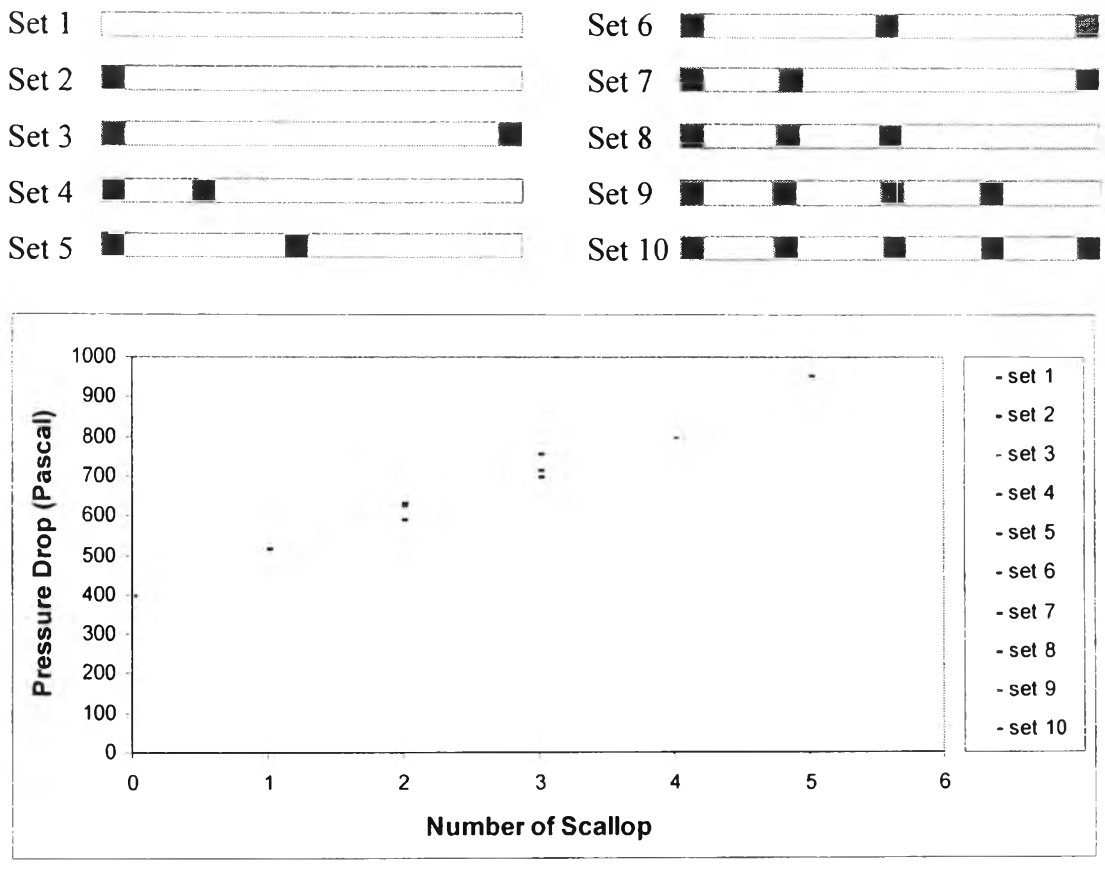

9 GPM

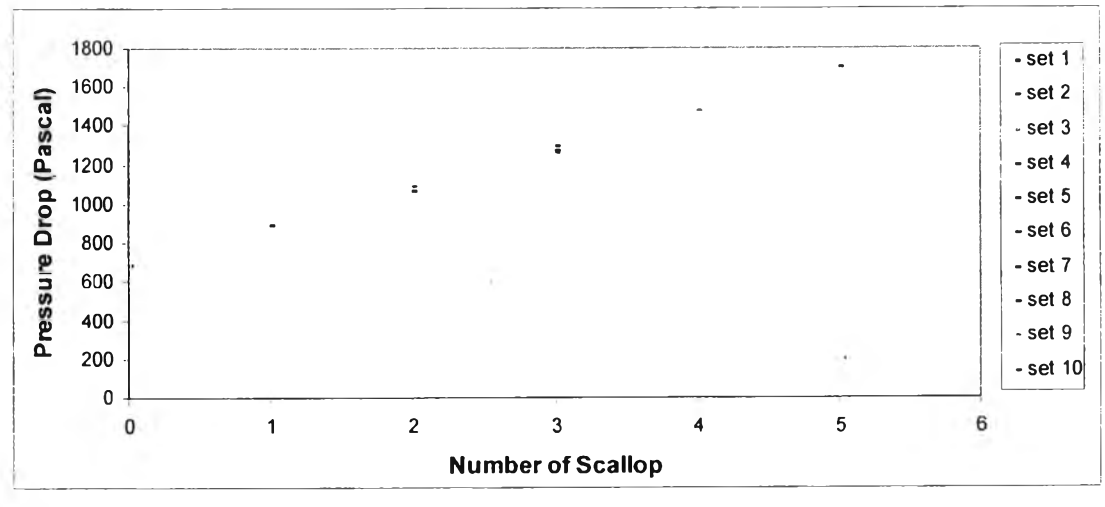

12 GPM

Figure 4.28 At the same numbers of scallops, the pressure drop is the almost the same regardless the scallop's distribution.